Numerical Simulation of Hydraulic Frac-turing Process for an Iranian Gas Field in the Persian Gulf

Mehran Kalhori[1]*, Ali Rafiee[1] and Hassan Eshraghi[2]

1. Mining Engineering Group, University of Zanjan, Iran
2. Pars Oil and Gas Company

(Received 2017.02.07, Accepted 2017.06.17)

Abstract

Most of the Iranian oil and gas wells in the Persian Gulf region are producing through their natural productivity and, in the near future, the use of stimulation methods will be undoubtedly necessary. Hydraulic fracturing as a popular technique can be a stimulation candidate. Due to the absence of adequate research in this field, numerical simulation can be an appropriate method to investigate the effectiveness of hydraulic fracturing. In the current study, the hydraulic fracturing process is simulated for a wellbore in the Persian Gulf region with Abaqus software. The main parameters that are necessary for the simulation are collected through wellbore logs and core tests. Fracturing process is studied with more emphasis on the pressure of fracturing fluid and fracture opening. Finally, several 3D fluid-solid coupling finite element models are generated and the main obtained results are compared.

Keywords

Hydraulic fracturing;
Finite Element Method;
Persian Gulf; Abaqus;
3D fluid-solid model.

1. Introduction

Hydraulic fracturing is a powerful technology that is being used in the petroleum industry in order to increase the inflow into wellbore in low permeability formations [1]. It is a process that the pore pressure build-up, for instance by an injection well, becomes sufficiently high to fracture the rock [2]. Hydraulic fracturing began in the oil and gas industry during the 1930s [3].

At the present time, hydraulic fracturing is widely used to improve the productivity of oil and gas wells. In production wells drilled in North America since the 1950s, about 70% of gas wells and 50% of oil wells have been hydraulically fractured [4]. Thousands of treatments are successfully pumped each year in various ranges of geological formations, e.g., low permeability gas fields, weakly consolidated offshore sediments, soft coal beds for methane extraction, naturally fractured reservoirs, and geometrically complex structures such as lenticular formations [5].

In the Persian Gulf region, there have been cases of hydraulic fracturing treatment in recent years [6-10]. But, this is not a usual way to enhance the productivity of wells in Iran; therefore, most of

* Corresponding Author.
Tel./Fax: +989197912131
Email address: mehrankalhori@znu.ac.ir (M. Kalhori)

the Iranian oil and gas wells produce by their natural flow potential. Over time, the reservoir pressure depletes and it is necessary for resorting to methods of stimulation. The lack of studies in this case could be the real reason not to use hydraulic fracturing as a method of stimulation. Obviously, it should be noted that hydraulic fracturing is a complex process and must be accurately studied to obtain satisfactory results. There are cases that the hydraulic fracturing fails due to lack of basic and primary studies on wellbore [11]. Hence, experimental and computational studies are needed to characterize mechanical and petrophysical properties of reservoir formations.

Hydraulic fracturing is complicated to model, even in its basic form, as it involves at least four processes [5-12]: (1) the mechanical deformation induced by the fluid pressure on the fracture surfaces; (2) the flow of fluid pressure on the fracture surfaces; (3) the fracture propagation; and (4) the leak-off of fluid from the fracture into the rock formation. Therefore, hydraulic fracturing requires interaction between 4 individual phenomena:

1) Porous medium deformation,
2) Pore fluid flow,
3) Fracturing fluid flow,
4) Fracturing propagation.

The following constitutive relations control the processes. For porous media, Biot's theory of poroelasticity, Darcy's Law for pore fluid flow, Reynold's lubrication theory for fracturing fluid flow, and the cohesive zone model to characterize fracturing are used. More information about Biot's theory and Darcy's Low is available in the references [13, 14]. The other cases are described in Section 4.

Numerical simulation of hydraulic fracturing process is important in order to understand the complicated mechanics of this technique that can be used for its efficient application as a stimulation method.

The first simplified forms of theoretical models for hydraulic fracturing were developed in the 1950s [15-17]. One of the great works in this era was a study conducted by Perkins and Kern [18], who adapted the classic elasticity plane-strain crack solution [19] to establish the so-called PK model. Later, Nordgren modified the PK model to devise the PKN model, which included the effects of fluid loss [20]. Afterwards, Khristianovic and Zheltov [21] and Geertsma and de Klerk [22] independently developed the so-called KGD (plane strain) model. Daneshy [23] extended the KGD model for the case of power-law fluids and, later, Spence and Sharp [24] introduced fracture toughness into the model. In recent years, there has been significant advancement in the numerical modeling of hydraulic fracturing in 2D and 3D models. 2D model of Hydraulic fracturing has been studied by Riahi et al.; by the use of UDEC, based on distinct-element, they showed that during early stages of hydraulic fracturing operation, low injection rates were more appropriate, because they provided a comparatively uniform aperture increase independent of fracture orientation [25]. 3D model of hydraulic fracturing was studied by Shimizu et al. with a model of PFC3D, based on assemblage of grains. Contacts of the grains have normal and shear forces, which allow to study breaking and slip. Their study showed that initiation pressure of the fracture with low-viscosity fluid was lower than that with high-viscosity fluid and when the high-viscosity fluid was used, the fracturing fluid would infiltrate along the existing straight fracture; therefore, thick and planar fracture with few branches were generated [26]. A 3D finite element model with ANSYS software was modeled by Huang et al. Their study considered fracture initiation region and propagation direction during hydraulic fracturing under different in-situ stresses. They showed that high lateral stress coefficient was conductive to create new compressive fractures instead of shear fractures [27]. More studies are available in the following references [5, 28-38].

The cohesive zone finite element method, which has its origin in the concept of a cohesive zone model for fracture, originally proposed by Dugdale and Barenblatt, has been widely used with successful results in simulation of fracture and fragmentation processes for concrete, rock, and ceramics [39, 40]. In this study, a full fluid-solid coupling 3D finite element model is proposed and cohesive element is used to simulate the propagation of a hydraulic fracture. Hydraulic fracturing process is simulated by using finite element method in order to demonstrate that this technique can be a proper and applicable method for stimulation of the tight gas wells in the Persian Gulf region. However, this study focuses essentially on geomechanical investigation and numer-

ical analysis; and, for performing hydraulic fracturing, it is obvious that further tests are needed and should be carried out particularly on reservoir rocks and fracturing fluid.

There are many parameters that affect the final result of hydraulic fracturing. Some of them depend on the instinctive properties of the rock, such as lithology, porosity, permeability, mechanical parameters, state of stress in the region, magnitude of stress, natural fractures, etc. These parameters cannot be controlled. On the other hand, there are design parameters which can be used for optimizing the HF operation. Among them are fracturing fluid and proppant selection, maximum allowable pump rate, injection steps, perforations orientation, etc.

2. Lithology of the Studied Section

Due to the influence of geological formations and their mechanical properties on the design and obtained results of numerical models, it is tried to briefly explain the lithology of the region here. Numerous giant gas and condensate fields have been discovered in the Persian Gulf Basin since the 1970s. Most of these fields produce from the Dalan (Permian) and Kangan (Triassic) formations. The reservoir rocks are regionally extensive in the subsurface Arabian plate and crop up in the Zagros Mountains, Central Arabian Arch, and the central and northern Oman Mountains (Fig. 1.a). The Kangan/Dalan reservoir dates back to the large-scale transgressive–regressive cycle of the middle upper Permian to lower Triassic. This formation is divided into four layers (K1 to K4), where 3 main lithologies (limestone, dolomite, and anhydrite) are alternating (Fig. 1.b). Anhydrite acts as a plugging element to the reservoir pores in the limestone and dolomite layers. The Kangan Formation is directly overlain by the Aghar shale, which is the actual seal of the hydrocarbon accumulation. The Dalan Formation is underlain by the clastic/shale Faraghan Formation [41]. For more details about lithology, tectonic, and geology of the study area, the interested reader can refer to [42, 43].

3. Geomechanical Parameters

3.1. Stress direction

One of the most critical parts of any project in geomechanical field is stress direction analysis. There are many parameters which affect the result of operation of hydraulic fracturing. Knowledge of stress direction helps to optimize the design of perforation for hydraulic fracturing process. Hydraulic fractures in rock always propagate perpendicular to the orientation of the minimum principal stress, because it is the least energy configuration. Thus, it is recommended that perforations be along maximum principle stress. Perforations that are not aligned with the maximum stress can result in complex flow path near the wellbore, which causes additional friction and pressure drops. This can result in proppant bridging and less optimal hydraulic fracturing treatment. There are several methods for identifying stress directions, including borehole breakout orientation, induced fracture orientation, shear-wave anisotropy measurements, and three-component VSP. In this study, the directions of principal stresses are analyzed using the orientations of occurred breakout on the wellbore wall.

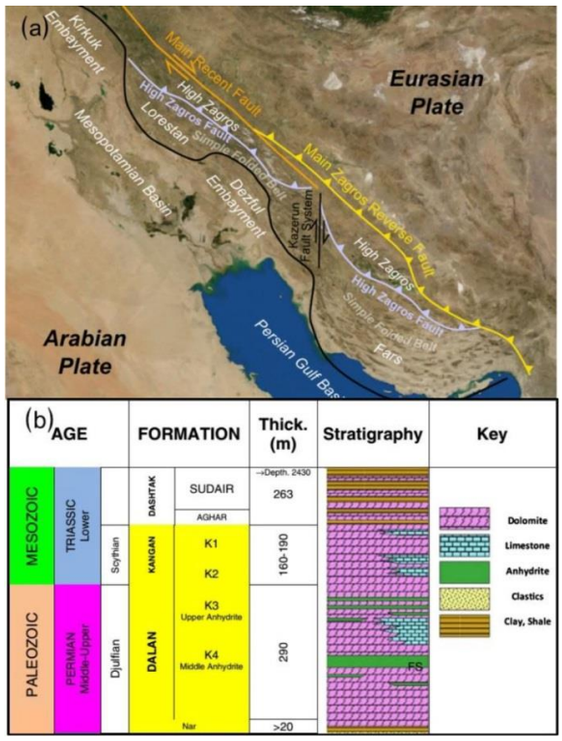

Figure 1. a) Geology and tectonics of Zagros belt, **b)** Stratigraphy of the Kangan/Dalan Formation in the Persian Gulf region [41]

Breakout generally occurs in the direction of minimum principal stress around the wellbore,

where there is the greatest stress concentration. Therefore, the direction of borehole breakout in a vertical wellbore indicates the minimum horizontal stress direction. Wellbore breakout direction can be determined from the image logs or the multi-arm caliper data. 41 Borehole breakouts are observed in the studied well, almost in the whole interval. The large majority of these elliptical breakouts have their longer axis oriented in almost NW-SE direction, which indicates that the orientation of apparent minimum horizontal stress S_{hmin} around the well is almost NW-SE. Therefore, the optimized direction for perforating is NE-SW (Fig. 2) (orientation of apparent maximum horizontal stress).

Considering world stress map, the dominant stress regimes of the area are reverse and strike-slip faulting in the Anderson classification of tectonic stress (Fig. 3). More information about stress of the area is available in a study by Haghi et al. [41].

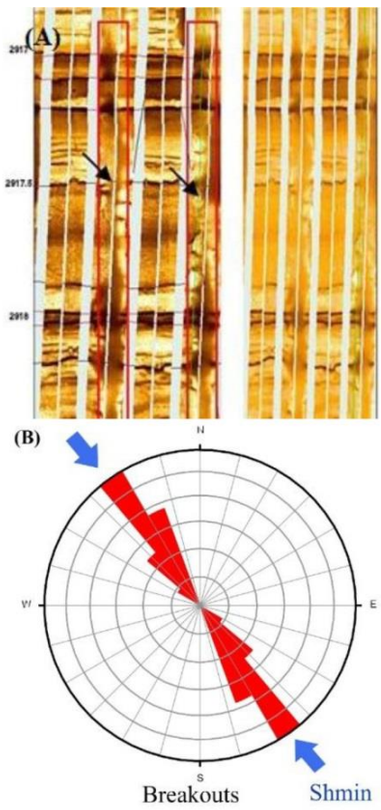

Figure 2. a) FMI image of the occurred breakouts in the study wellbore, **b)** orientation of the occurred breakouts on the wellbore wall

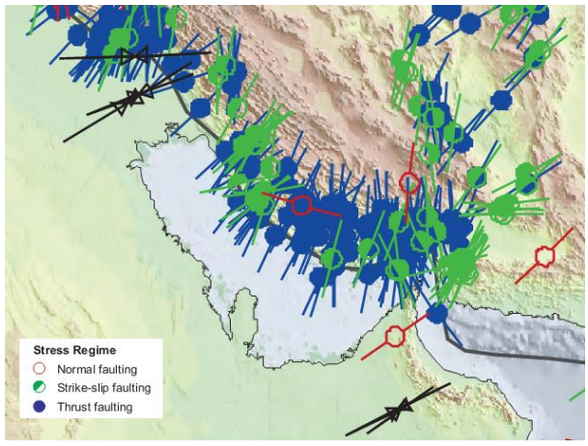

Figure 3. Stress map of the Persian Gulf [44]

3.2. Stress magnitudes

Vertical stress magnitude

The vertical stress magnitude at a specified depth is commonly assumed to be the pressure exerted by the overlying rocks. Vertical stress S_v is computed by integrating formation density ρ from surface into TD using the following formula:

$$S_v = \int_0^z \rho(z).g.dz \quad (1)$$

Horizontal stresses magnitudes

Stress state in this region has recently been studied by Haghi [41]. The study has shown that there is a strike-slip fault stress regime in Dalan/Kangan formation and the minimum horizontal stress S_{hmin} gradient is $2.5psi/m$ in the formation. This magnitude is confirmed by three Leak-off tests (LOT) in depths of 2325, 2497, and 2618m of the study well. As shown in Fig. 4, there is about 435psi difference between LOT results and calculated S_{hmin} for the formation, which can be regarded to be in an acceptable range.

To calculate the magnitude of maximum horizontal stress, tensile fracture formation in the wellbore and related empirical formulae are used. These conditions by considering tensile fracture formation are placed in Kirsch formula, resulting in the following equation [45, 46]:

$$S_{Hmax} = 3S_{hmin} - 2P_p - \Delta P - T_0 - \sigma^{\Delta T} \quad (2)$$

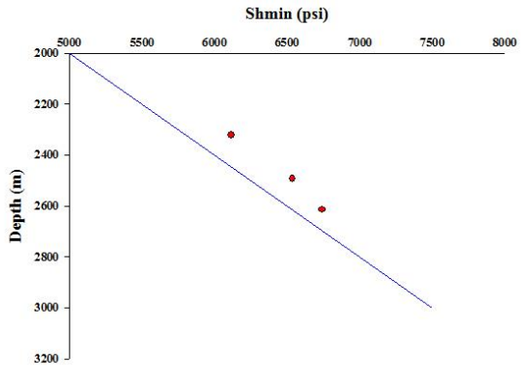

Figure 4. Comparison between LOT results and available values for minimum horizontal stress

where, $\sigma^{\Delta T}$, T_0, and ΔP are cooling stress, tensile strength, and excess mud weight, respectively. $\sigma^{\Delta T}$ and T_0 are quite small and negligible. By considering ΔP and/or neglecting it, a lower and/or an upper bound can be estimated for S_H.

On the other hand, the magnitude of maximum horizontal stress in strike-slip fault regime is also related to the minimum horizontal stress with the following formula [47]:

$$\frac{S_{Hmax}-P_p}{S_{hmin}-P_p} \leq \left[(\mu^2+1)^{1/2}+\mu\right]^2 \quad (3)$$

where μ is coefficient of friction and, with considering $\mu = 0.6$, there is an upper bound of S_{Hmax}.

$$S_{Hmax} \leq 3.1S_{hmin} - 2.1P_p \quad (4)$$

These equations are used for determining the magnitude of S_H as well as constraining its variation range.

Pore pressure

Pore pressure is calculated through resistivity method, and is calibrated by RFT results. Gradient of pore pressure in the studied interval of the wellbore is determined to be 1.9psi/m.

The total trends of stresses and pore pressure are shown in Fig. 5.

3.3. Rock property in the studied interval

The variations of porosity and permeability in the study interval are obtained from core analysis. In depth range of 2815-2818m, the permeability has an average of 380mD, which shows a high permeability and from 2818m to 2848m, it decreases to an average of 26mD; moreover, in the depth of 2848-2850m, there is an increase in permeability value to 232mD. Porosity, with an average of 19%, varies between 3% and 25% in the main part of the studied interval (Fig. 6).

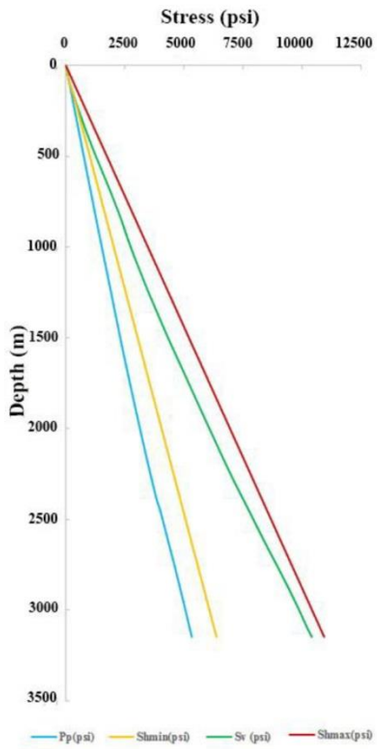

Figure 5. Trend of changes in stress amounts and pore pressure in the wellbore

Dynamic elastic moduli and Poisson's ratio of rock are calculated based on compressional and shear wave travel times (Fig. 7) [48, 49].

$$\nu_{dyn} = \frac{1/2\left(\frac{\Delta t_s}{\Delta t_c}\right)^2-1}{\left(\frac{\Delta t_s}{\Delta t_c}\right)^2-1} \quad (5)$$

$$E_{dyn} = \frac{\rho_b\left[3-4\left(\frac{\Delta t_c}{\Delta t_s}\right)^2\right]}{\Delta t_s{}^2-\Delta t_c{}^2} \quad (6)$$

where Δt_s is velocity of shear waves in $\frac{s}{km}$, Δt_c is velocity of compressional waves in $\frac{s}{km}$, and ρ_b represents density in $\frac{gr}{cm^3}$.

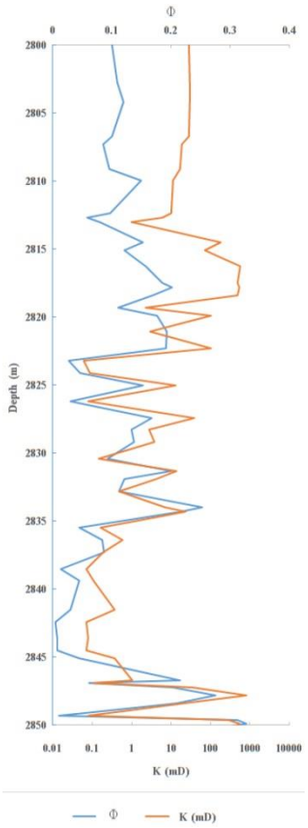

Figure 6. Variations of porosity and permeability for the studied interval

For this study, both compressional and shear waves data are provided directly from well logs. The dynamic elastic modulus can be converted into static modulus by empirical correlations. It should be mentioned that data for five core tests are available, and they are used to calibrate the calculated values. In the studied interval of the formation, permeability in the depth range of 2820m to 2840m is partially constant and low. As a result, the numerical analysis of hydraulic fracturing process is decided to be performed in this interval of the wellbore.

4. Simulation of Hydraulic Fracturing

In this study, cohesive element structure is used in order to simulate the behavior of generated fracture in the wellbore wall. In other words, a pre-defined surface made up of elements that support the cohesive zone with traction-separation calculation is embedded in the rock and the hydraulic fracture grows along this surface. The available traction-separation in the model assumes initially linear elastic behavior followed by the initiation and evolution of damage. The elastic behavior is written in terms of an elastic constitutive matrix that relates the nominal stresses to the nominal strains across the interface. The nominal stresses are the force components divided by the original area at each integration point, while the nominal strains are the separations divided by the original thickness at each integration point. The nominal traction stress vector t consists of three components t_n, t_s, and t_t, which represent the normal and the two shear tractions, respectively. The corresponding separations are denoted by δ_n, δ_s, and δ_t. The nominal strains can be defined as:

$$\varepsilon_n = \frac{\delta_n}{T_0}$$
$$\varepsilon_s = \frac{\delta_s}{T_0} \qquad (7)$$
$$\varepsilon_t = \frac{\delta_t}{T_0}$$

where T_0 is the original thickness of the element.

$$t = \begin{bmatrix} t_n \\ t_s \\ t_t \end{bmatrix} = \begin{bmatrix} K_{nn} & 0 & 0 \\ 0 & K_{ss} & 0 \\ 0 & 0 & K_{tt} \end{bmatrix} \begin{bmatrix} \varepsilon_n \\ \varepsilon_s \\ \varepsilon_t \end{bmatrix} = K\varepsilon \qquad (8)$$

where K is stiffness of matrix K_{nn}, K_{ss} and K_{tt} are stiffness components.

However, once the traction in a cohesive element reaches the damage initiation value, material damage occurs according to a damage evolution law. The traction acting on cohesive element monotonically degrades as the separation displacement between the two outer surfaces of cohesive element increases after damage initiation.

Damage initiation refers to the beginning of degradation of the response of a material point. The process of degradation begins when the stresses and/or strains satisfy certain damage initiation criteria that have been specified. Several damage initiation criteria are available. Here, quadratic nominal stress criterion has been used in which damage is assumed to initiate when a quadratic interaction function involving the nominal stress ratios (as defined in the expression below) becomes equal to one. This criterion can be represented as [50]:

$$\{\frac{\langle t_n \rangle}{t_n^o}\}^2 + \{\frac{\langle t_s \rangle}{t_s^o}\}^2 + \{\frac{\langle t_t \rangle}{t_t^o}\}^2 = 1 \qquad (9)$$

where $\boldsymbol{t_n}$, $\boldsymbol{t_s}$, and $\boldsymbol{t_t}$ represent the normal and two shear tractions, respectively. $\boldsymbol{t_n^o}$, $\boldsymbol{t_s^o}$, and $\boldsymbol{t_t^o}$ represent the tensile strength and shear strengths in corresponding directions, respectively. The symbol ‹› represents the Macaulay bracket with the usual interpretation. Macaulay brackets are used to signify that a pure compressive deformation or stress state does not induce damage.

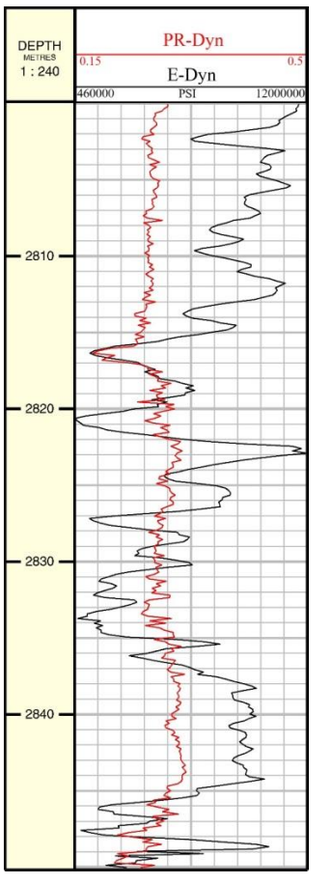

Figure 7. Variations of dynamic elastic modulus and Poisson's ratio for the studied interval of the wellbore

The damage evolution law describes the rate at which the material stiffness is degraded once the corresponding initiation criterion is reached. A scalar damage variable D represents the overall damage in the material and captures the combined effects of all the active mechanisms. It initially has a value of 0. If damage evolution is modeled, D monotonically evolves from 0 to 1 upon further loading after the initiation of damage. The stress components of the traction-separation model are affected by the damage according to [51]:

$$t_n = \begin{cases} (1-D)\bar{t}_n\,,\ \bar{t}_n \geq 0 \\ \bar{t}_n\,,\ otherwise \\ (no\ damage\ to\ compressive\ stiffness) \end{cases}$$

$$t_s = (1-D)\bar{t}_s$$

$$t_t = (1-D)\bar{t}_t \qquad (10)$$

where $\bar{t}_n$, $\bar{t}_s$, and $\bar{t}_t$ are the stress components predicted by the elastic traction-separation behavior for the current strains without damage.

The damage evolution for mixed mode failure is defined based on B-K fracture criterion [52]:

$$G_C = G_{IC} + (G_{IIC} - G_{IC})\left(\frac{G_{IIC}+G_{IIIC}}{G_{IC}+G_{IIC}+G_{IIIC}}\right)^{\eta} \qquad (11)$$

where G_{IC}, G_{IIC}, and G_{IIIC} are fracture critical energy release rates for mode I (tensile or opening mode), mode II (in-plane shear or sliding mode), and mode III (anti-plane shear or tearing mode).

Fluid flow within cohesive zone

It should be noted that the fluid constitutive response comprises:

1) Tangential flow within the gap,
2) Normal flow across the gap.

The flow patterns of the pore fluid in the element are shown in Fig. 8.

The fluid is assumed to be incompressible and the formulation is based on a statement of flow continuity that considers tangential and normal flows as well as the rate of opening of the cohesive element. The tangential flow within the gap is [52]:

$$qd = -\frac{d^3}{12\mu}\nabla p \qquad (12)$$

where d, μ, and ∇p respectively represent gap opening, the fluid viscosity, and the pressure gradient along the cohesive element.

The normal flow is defined as [51]:

$$q_t = c_t(p_i - p_t) \qquad (13)$$

$$q_b = c_b(p_i - p_b) \qquad (14)$$

c_t And c_b are leak-off coefficients for top and bottom surfaces, q_t and q_b are the flow rates into the top and bottom surfaces, respectively, and p_i is internal pressure.

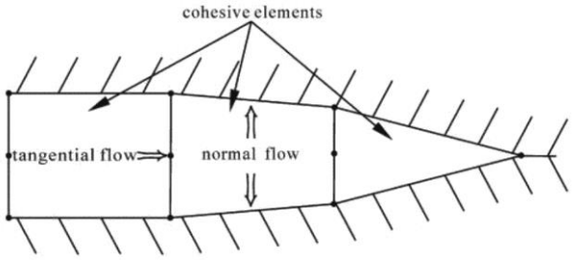

Figure 8. Fluid flow in cohesive elements considering both tangential and normal flows [51]

5. Modeling

Hydraulic fracturing is simulated in the formation at true vertical depth (TVD) between 2810m and 2850m. A semi-circular layer with radius of 400m and thickness of 40m is used for simulating this portion of the reservoir. Because of existing symmetry in the model, a half of the total shape is only modeled. The locality of anticipated crack generated by hydraulic pressure is considered to be in the central part of the semicircle. A set of cohesive elements (COH3DP), which have pore pressure as the primary nodal variables, is used to simulate the fracture. Perforation, wellbore, and steel linear are also included in the model. The reservoir rock is modeled with C3D8RP elements and M3D4 elements are considered for the wellbore linear. Displacement constraints are applied to the outer and bottom surfaces of the model. The boundary conditions of pore pressure are assumed constant and are of the same values as those used for the initial pore pressure. Mohr-Coulomb criterion is used for different parts of the reservoir rock and the linear is assumed to have elastic behavior. Fluid leak-off coefficient is specified as 5e-13m/Pa.s for top and bottom surfaces of the cohesive elements. The gap flow is considered Newtonian with a viscosity of 0.001Pa.s. A summary of mechanical properties considered for rock and fracture modeling is provided in Tables 1 and 2.

The investigation consists of two phases; in the first step, a basic model is solved and its results are analyzed. Later, five models with the same properties of the basic model but with different injection rates are solved and the results are compared.

The numerical analysis consists of three steps briefly described below. Firstly, after applying the initial pore pressure to the formation and the initial in-situ stresses, a geostatic step is performed to reach an equilibrium state. The second phase is hydraulic fracturing process in which the main volume of fluid is injected into the well for 30min. Various values for injection time and fluid rate have been tried to get optimum fracture. There is a cutoff for time by which increasing the injection time is ineffective, and this is where all the injecting fluid leaks into the target formation. In the last step, the injection is stopped and an additional boundary condition is applied to simulate the behavior of the proppant material that was injected into the fracture.

Table 1. Parameters used for cohesive zone

Elastic Parameters (psi)	K_{nn}	K_{ss}	K_{tt}
	12328204	12328204	12328204
Damage ignition Quads (psi)	t_n^o	t_s^o	t_t^o
	116	1740	1740
Damage Evolution Energy (N/m)	G_{IC}	G_{IIC}	G_{IIIC}
	70	1000	1000

Table 2. Mechanical properties of reservoir rocks

Depth (m)	Cohesion (psi)	Friction angle (deg)	Young's Modulus (ksi)	Poisson's Ratio
2810-2820	1273	48.1	4081.4	0.189
2820-2840	2079	39.6	3125.6	0.193
2840-2850	2717	32.2	3340.2	0.197

To study the effect of injection rate changes on fracture aperture and fracture propagation, the created model has been used. The only thing that has changed is the injection rate and all the parameters and conditions are as clarified before. Therefore, five hydraulic fracturing models with different injection rates are simulated. The fracture surface and fracture aperture are compared for different injection rates. Fracturing process is investigated for injection rate of 4bpm.

Modeling results

In this part of the study, it is attempted to present some of the results obtained by numerical model-

ing using the parameters described previously. Fig. 9 shows the well pressure (at the injection point) as a function of time. This figure illustrates that the propagation of fracture is a multistage process, whereby a number of elements is broken in each phase. It should be noted that volume of fluid in the fracture is same as it was just before immediately after fracture occurs. As the propagation of the fracture leads to a larger fracture surface, a lower fluid pressure is required to keep the fracture open. On the other hand, it should be taken into account that a constant fluid volume in the fracture, which is associated with an increasing fracture surface, provides a reduced fracture aperture. As a result, by considering all the above explanations, an instantaneous fluid pressure drop occurs in the fracture during its growth. It should also be mentioned that the injection point is a pre-fractured element and high pressure is required to fracture the neighbors of the first element relative to the pressure needed to propagate the rest of the fracture. The initial fracture becomes larger when the closest neighbor elements break; consequently, this significant expansion of the fracture leads to a pressure loss.

The pressure and opening curves for special points on the fracture surface are shown in Fig. 9.

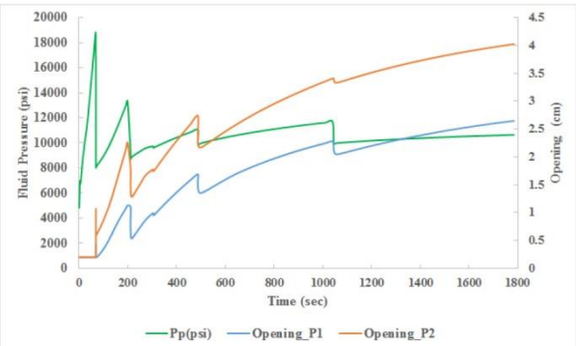

Figure 9. Variation of fluid pressure at injection point and aperture width in two different points at the wellbore wall

The fracture aperture variation is also shown in Fig. 9 for two different points located on the fracture surface, which is exposed to the injected fluid. As can be seen, the openings of the fractures are different for these two points. The opening width is a function of the distance of concerned point from the point of perforation, which is exposed to the maximum amount of fluid injection pressure and, evidently, the maximum calculated value for aperture. Despite different opening widths over the fracture surfaces on the wellbore wall, the mechanism of fracture propagation is the same for the nodes close to the perforation point. As shown in the graph (Fig.9), five incremental steps for opening width can be distinguished, which are consistent with the fluid pressure-time curve. When fluid is being injected, the fluid pressure quickly increases, because there is not enough space for injecting fluid to scape; thus, the fracture is simultaneously initiated to open until the fluid pressure surpasses rock tensile strength as well as minimum principle stress, where the fracture breakdown pressure occurs. From this point, the fracture propagation starts. Normally, at this point, the fluid pressure begins to drop rapidly, indicating that volume of the fracture is increased and, due to the pressure drop, the fracture opening width is reciprocally reduced. This process is repeated in five stages during the injection for both the fracture opening width and the fluid pressure (Fig. 9). Fig. 10 shows the generated fracture on the wellbore wall.

The numerical analysis is performed for 5 different injection rates, by considering that all the models have similar conditions including fracturing fluid viscosity, injection time, and other affecting parameters. The main selected parameters, on which this part of the study is focused, are the surface of generated fractures and the average opening width. As can be extracted from the obtained results, the fracture surface is increased with the higher injection rate (Table 3). For the cases with injection rates of 3 and 4bpm, the surfaces of the fracture are approximately equal while the fracture aperture determined for the injection rate of 4bpm is about 1.5 times the other one. Finally, by increasing the injection rate to 5bpm, the amount of fracture surface increases but the fracture aperture is lower than that in the case with injection rate of 4 bpm.

6. Conclusion

In the current study, a gas wellbore in the Persian Gulf region is numerically investigated in order to verify the possibility of using hydraulic fracturing technique. For simulation of hydraulic fracturing process, different types of parameters are re-

quired. Some of these data can be directly measured and others should be extracted from the field condition and available data. The porosity and permeability are determined from available core data and the mechanical properties of the reservoir rock are extracted from the velocity measurements of compressive and shear waves and, then, they are calibrated with the core test database.

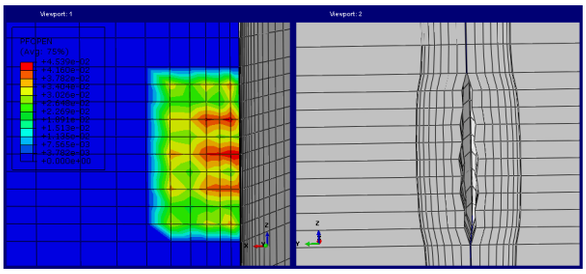

Figure 10. Fracture opening and close-up image of the fracture opening magnified 50 times

Table 3. Obtained results for different injection rates

Case	Injection rate (bpm*)	Average aperture of fracture (cm)	Fracture surface (m²)
1	1	3.1247	19.60
2	2	2.4135	106.40
3	3	2.0391	186.32
4	4	3.3012	192.43
5	5	2.3348	326.23

*bpm: barrel per minute

The state of in-situ stresses is one of the main influencing parameters in hydraulic fracturing process. The vertical stress is determined from density of overlaying rock at each depth. The value of minimum horizontal stress is determined for the formation and is confirmed by available LOT results. The maximum horizontal stress is constrained by tensile fracture formation, pore pressure measurements, and the determined minimum horizontal stress. It should be noted that to obtain satisfactory results from numerical simulation, it is necessary to have access to high quality input data. A 3D model for hydraulic fracturing process simulation is established by Abaqus software and all collected data are taken into account in the model.

Although it may be argued that the results obtained from numerical modeling may not conform to reality, simulated process showed acceptable and logical outcomes. This study allowed investigating the structure of a generated fracture from different aspects such as propagation mechanism, variation of the fracture aperture, and the surface of fracture. The effects of different injection rates on the aperture size and the surface of generated fracture are also studied. All achieved results can be used to regulate the injection rate and to choose a proper proppant in order to obtain a hydraulically generated fracture with appropriate and acceptable dimensions. Many studies are necessary to successfully perform this process, but the results show that this technique can be a promising method for the stimulation of the tight reservoirs in the Persian Gulf region.

Nomenclature

E Young modulus
c_t Leak-off coefficients for top surface
c_b Leak-off coefficients for bottom surface
D Damage, variable from 0 to 1
d Gap opening
G_{IC} Critical energy release for mode I (tensile or opening mode)
G_{IIC} Critical energy release for mode II (in-plane shear or sliding mode)
G_{IIIC} Critical energy release for mode III (anti-plane shear or tearing mode)
g Gravity (9.81 m/s^2)
K Permeability (mD)
K Stiffness
P_p Pore pressure
q Flow rate (m^3/sec)
S_{Hmax} Maximum horizontal stress
S_{hmin} Minimum horizontal stress
S_v Vertical stress
T_0 Tensile strength
t Traction stress vector
z Depth (m)
ΔP Difference of mud weight and pore pressure
Δt_s Velocity of shear waves
Δt_c Velocity of compressional waves
δ Separation
ε Strian
μ Fluid viscosity (mPa.s)
μ Coefficient of friction, usually equal to 0.6
ν_{dyn} Dynamic Poisson's Ratio
ρ Density (Kg/m^3)
$\sigma^{\Delta T}$ Cooling stress
Φ Porosity

Acknowledgement

The first author of this purely scientific study is grateful to the Pars Oil and Gas Company (POGC) for supporting and data sharing.

References

1. Bohloli, B., and Pater, C.J. (2006). "Experimental study on hydraulic fracturing of soft rocks: Influence of fluid rheology and confining stress." *Journal of Petroleum Science and Engineering*, Vol. 53, pp.1-12.
2. Jaeger, J., Cook, N., Zimmerman, R. (2007). *Fundamentals of Rock Mechanics*. 4th Ed., Blackwell Scientific Publications.
3. Grebe, J. and Stoesser, M. (1935). "Increasing crude production 20,000,000 bbl." *World Petroleum J*, pp. 473–82.
4. Valkó, P., and Economides, M. (1995). *Hydraulic Fracture Mechanics*. Wiley.
5. Adachi, J., Siebrits, E., Peirce, A., Desroches, J. (2007). "Computer simulation of hydraulic fractures." *International Journal of Rock Mechanics & Mining Sciences*, Vol. 44, pp. 739–757.
6. Lee, B., Soleimani, A., Dyer, S. (2009). "Optimization of Multiple Hydraulic Fractures for Open Hole Horizontal Wells by Numerical Modeling-Saudi Arabia case study." *SPE-124406-MS*.
7. Rahim, Z., AL-Kanaan, A., Johnston, B. (2011). "Success Criteria for Multistage Fracturing of Tight Gas in Saudi Arabia." *SPE-149064-MS*.
8. Alzarouni, A., and Ghedan, S. (2012). "Paving the road for the first Hydraulic Fracturing in Tight Gas Reservoirs in Offshore Abu Dhabi." *SPE-152713-MS*.
9. Alexyenko, A., Bartko, K., Adebiyi, I., Faraj, O. (2013). "Reduced Polymer Loading, High Temperature Fracturing Fluids using Nanocrosslinkers." *SPE-177469-MS*.
10. Bartko, K., Salim, A., Saldungaray, P., Kalinin, D., Han, X., Saldungaray, P. (2013). "Hydraulic Fracture Geometry Evaluation Using Proppant Detection: Experiences in Saudi Arabia." *SPE-168094-MS*.
11. Rahman, M., Suarez, Y., Chen, Z., Rahman, S. (2007). "Unsuccessful hydraulic fracturing cases in Australia: Investigation into causes of failures and their remedies." *Journal of Petroleum Science and Engineering*, Vol. 57, pp. 70-81.
12. Bunger, A., Detournay, E., Garagash, D. (2005). "Toughness-dominated hydraulic fracture with leak-off." *International Journal of Fracture*, Vol. 134 (2), pp. 175-190.
13. Kundu, P., Kumar, V., Mishra, M. (2016). "Experimental and numerical investigation of fluid flow hydrodynamics in porous media: Characterization of Darcy and non-Darcy flow regims." *Powder Technology*, Vol. 303, pp. 278-291.
14. Fjaer, E., Holt, R., Horsrud, P., Raaen, A., Risnes, R. (2008). *Petroleum Related Rock Mechnaics*. 2th Ed., Elsevier.
15. Harrison, E., Kieschnick, W., McGuire, W. (1954). "The mechanics of fracture induction and extension. Petroleum Trans." *AIME*, pp. 252-263.
16. Hubbert, M., Willis, D. (1957). "Mechanics of hydraulic fracturing." *Journal of Petroleum Technology*, Vol. 9(6), pp. 153-168.
17. Crittendon, B. (1959). "The mechanics of design and interpretation of hydraulic fracture treatments." *SPE-1106-G*.
18. Perkins, T.K. and Kern, L.R. (1961). "Widths of hydraulic fractures." *SPE 89*, pp. 937-949.
19. Sneddon, I. and Elliot, H.A. (1946). "The opening of a Griffith crack under internal pressure." *Q Appl Math,* Vol. 4, pp. 262–7.
20. Nordgren, R. (1972). "Propagation of a vertical hydraulic fracture." *SPE Journal*, Vol. 12(8), pp. 306-314.
21. Khristianovic, S.A. and Zheltov, Y.P. (1955). "Formation of vertical fractures by means of highly viscous liquid." *Proc. 4th world petroleum congress, Rome*, pp. 579–86.
22. Geertsma, J. and de Klerk, F.A. (1969). "Rapid method of predicting width and extent of hydraulically induced fractures." *Journal of Petroleum Technology*, Vol. 21, pp. 1571–81.

23. Daneshy, A.A. (1973). "On the design of vertical hydraulic fractures." *SPE 3654*.

24. Spence, D.A. and Sharp, P. (1985). "Self-similar solutions for elastohydrodynamic cavity flow." *Proc R Soc London A*, pp.289–313.

25. Riahi, A., and Damjanac, B. (2013). "Numerical study of hydro-shearing in geothermal reservoirs with a pre-existing discrete fracture network." *Proceedings thirty-eighth workshop on geothermal reservoir engineering,* California: Stanford University, pp. 1-13.

26. Shimizu, H., Murata, S., Ishida, T. (2011). "The distinct element analysis for hydraulic fracturing in hard rock considering fluid viscosity and particle size disterbution." *International journal of rock mechanics and mining sciences*, Vol. 48, pp. 712-727.

27. Huang, S., Liu, D., Yao, Y., Gan, Q., Cai, Y., Xu, L. (2017). "Natural fractures initiation and fracture type prediction in coal reservoir under different in-situ stresses during hydraulic fracturing." *Journal of Natural Gas Science and Engineering*. doi:10.1016/j.jngse.2017.03.022

28. Advani, S. H., Lee, T. S., Lee, J. K. (1990). "Dimensional modeling of hydraulic fractures in layered media.1. Finite-element formulations." *Journal of Energy Resources Technology-Transactions of the ASME*, Vol. 112(1), pp. 1-9.

29. Valko, P., and Economides, M.J. (1994). "Propagation of hydraulically induced fractures- a continuum damage mechanics approach." *International Journal of Rock Mechanics and Mining Sciences & Geomechanics*, Vol. 31(3), pp. 221-229.

30. Ouyang, S., Carey, G.F., Yew, C.H. (1997). "An adaptive finite element scheme for hydraulic fracturing with proppant transport." *International Journal for Numerical Methods in Fluids*, Vol. 24, pp. 645-670.

31. Papanastasiou, P. (1999). "An efficient algorithm for propagating fluid-driven fractures." *Computational Mechanics*, Vol. 24, pp. 258-267.

32. Dong, C., Pater, C. (2001). "Numerical implementation of displacement discontinuity mothed and its application in hydraulic fracturing." *computer methods in apllied mechanics and engineering*, Vol. 191, pp. 745-760.

33. Zhang, X., Detournay, E., Jeffrey, R. (2002). "Propagation of a penny-shaped hydraulic fracture parallel to the free-surface of an elastic half-space." *International Journal of Fracture*, Vol. 115, pp. 125-158.

34. Lecamplon, B., and Detournay, E. (2007). "An implicit algorithm for the propagation of a hydraulic fracture with a fluid lag." *Computer Methods in Applied Mechanics and Engineering*, Vol. 196, pp. 4863–4880.

35. Peirce, A., and Detournay, E. (2008). "An implicit level set method for modeling hydraulically driven fractures." *Computer Methods in Applied Mechanics and Engineering*, Vol. 197, pp. 2858–2885.

36. Chen, Z., Bunger, A., Zhang, X., Jeffrey, R. (2009). "Cohesive zone finite element based modeling of hydraulic fractures." *Acta Mechanica Solida Sinica*, Vol. 22, pp. 443–452.

37. Dean, R., and Schmidt, J. (2009). "Hydraulic fracture predictions with a fully coupled geomechanical reservoir simulator." *SPE Journal*, Vol. 14, pp. 707-714.

38. Carrier, B., and Granet, S. (2012). "Numerical modeling of hydraulic fracture problem in permeable medium using cohesive zone model." *Engineering Fracture Mechanics*, Vol. 79, pp. 312-328.

39. Dugdale, D. (1960). "Yielding of steel sheets containing slits." *Journal of the Mechanics and Physics of Solids*, Vol. 8(2), pp. 100-104.

40. Barenblatt, G. (1962). "The mathematical theory of equilibrium of cracks in brittle fracture." *Advances in Applied Mechanics*, Vol. 5, pp. 55-129.

41. Haghi, A., Kharrat, R., Asef, M., Rezazadegan, H. (2013). "Present-day stress of the central Persian Gulf: Implications for drilling and well performance." *Tectonophysics,* Vol. 608, pp. 1429-1441.

42. Esrafili-Dizaji, B., and Rahimpour-Bonab, H. (2009). "Effects of depositional and diagenetic characteristics on carbonate reservoir quality: a case study from the South Pars gas field in the Persian Gulf." *Petroleum Geoscience*, Vol. 15, pp. 325–344.

43. Ziegler, M. (2001). "Late Permian to Holocene Paleofacies Evolution of the Arabian Plate and its Hydrocarbon Occurrences." *GeoArabia*, Vol. 6, pp. 455-504.

44. 2016. [Online]. Available: http://www.world-stress-map.org/download/.

45. Zoback, M. (2007). *Reservoir Geomechanics,* Cambridge University Press, New York.

46. Kirsch, G. (1898). *Die Theorie der Elastizitat und die Bedurfnisse der Festigkeitslehre. Zeitschrift des Verlines DeutscherIngenieure.*

47. Zoback, M., Barton, C., Brudy, M., Castillo, D., Finkbeiner, T., Grollimund, B., Wiprut, D. (2003). "Determination of stress orientation and magnitude in deep wells." *International Journal of Rock Mechanics & Mining Sciences*, Vol. 40, pp. 1049–1076.

48. Tixier, M.P., Loveless, G., Anderson, R. (1975). "Estimation of Formation Strength from the Mechanical-Properties log." *SPE 4532.*

49. Sethi, D.K. (1981). "Well log application in rock mechanics." *SPE 9833.*

50. Yao, Y., Gosavi, S., Searles, H., Ellison, T. (2010). "Cohesive Fracture Mechanics Based Analysis to Model Ductile Rock Fracture." *AR-MA-10-140*.

51. Zhang, G., Liu, H., Zhang, J., Wu, H., Wang, X. (2010). "Three-dimensional finite element simulation and parametric study for horizontal well hydraulic fracture." *Journal of Petroleum Science and Engineering*, Vol. 72, pp. 310–317.

52. Benzeggagh, and Kenane. (1996). "Measurement of mixed-mode delamination fracture toughness of unidirectional glass/epoxy composites with mixed-mode bending apparatus." *Composites Science and Technology*, Vol. 56, pp. 439–449.